International Journal of Pharmaceutics 408 (2011) 102–112

Contents lists available at ScienceDirect

International Journal of Pharmaceutics

journal homepage: www.elsevier.com/locate/ijpharm

# Theoretical and experimental investigations into the delamination tendencies of bilayer tablets

Fridrun Podczeck*

*Dept. Mechanical Engineering, University College London, Torrington Place, London WC1E 7JE, United Kingdom*

ARTICLE INFO

*Article history:*
Received 17 December 2010
Received in revised form 1 February 2011
Accepted 4 February 2011
Available online 21 February 2011

*Keywords:*
Bilayer tablets
Delamination
Elastic mismatch
Far field stress intensity factor
Fracture mechanics
Thermal stress

ABSTRACT

Delamination is one major problem in the production of layered tablets, yet there is little knowledge about the physical reasons for this to occur. The aim of this work was to explore the theoretical influence of thermal stresses and strains that can develop during tabletting and to devise an experimental method that can be used to detect delamination tendencies in bilayered tablets. Theoretical considerations have shown that thermal stresses due to development of heat during powder compaction can result in delamination, and this effect is the more pronounced the larger the Young's modulus for the individual layer materials is. Elastic mismatch further enhances delamination tendencies. Experiments on mixed powder beams showed that there is only limited adhesion between particle surfaces of a model drug (acetylsalicylic acid) and model excipient (lactose monohydrate), indicative of limited adhesion between similar interfaces in layered tablets. A three-point bending test was developed to determine the far field stress intensity factor for bilayered compacts. Under the test conditions employed, lactose monohydrate behaved as a brittle material, whereas acetylsalicylic acid demonstrated ductility, which resulted in considerable differences in the far field stress intensity factor values, depending on whether the excipient or the drug formed the downward facing layer during the bending test. Ductile phase toughening was observed when the drug formed the downward facing layer, and hence for bilayer tablets made from these two powders lactose monohydrate must form the downward facing layer during the test. Using the correct test configuration the far field stress intensity factor correctly predicted practically observed delamination between the two material layers. Hence, the proposed fracture mechanics approach could become a formulation tool in the development of bilayered tablets.



## 1. Introduction

The manufacture of multilayer tablets has been successful for over 50 years and one of the early scientific evaluations of layered tablets was published by Stephenson (1961). New machine designs developed during the late 60s have made it possible to check the weight of individual layers by sampling without stopping the machine, providing in-process control facilities to ensure correct dosing (Gunsel et al., 1970). However, despite this, a considerable amount of expertise is still required to formulate these tablets and to ensure consistent manufacture to satisfy regulatory requirements (Vaithiyalingam and Sayeed, 2010). One problem that causes great concern is the delamination of layered tablets (Wu and Seville, 2009), which has become a more obvious problem with the increase in compression speed on modern high-speed rotary machines. The formulations used for each individual layer should be compressible and compactable on their own i.e. they should show satisfactory reduction in volume and form mechanically strong, coherent solid bodies. Under this assumption the interface between the layers should weld together during compaction and strong adhesion forces should hold the layers together after tablet ejection. However, this is not always the case, and as compressibility and compactability of the individual layers should not be the cause for delamination, other physical mechanisms need to be identified that can explain the problems with delamination that have hampered recent developments of layered tablets. Inman et al. (2007) confirmed observations first made by Karehill et al. (1990), i.e. that the compaction pressure used to form the first tablet layer should be kept at a minimum to provide sufficient surface roughness for nesting and particle interlocking between layers to occur. Due to the increase in surface roughness there is a larger contact area between the layers, which enhances interlayer

*Abbreviations:* ASS, acetylsalicylic acid; ASS(t)/LM(c), ASS top layer, LM lower layer during compaction – notch in LM layer; ASS(t,c)/LM, ASS top layer, LM lower layer during compaction – notch in ASS layer (inverted beam); LM, lactose monohydrate; LM(t)/ASS(c), LM top layer, ASS lower layer during compaction – notch in ASS layer; LM(t,c)/ASS, LM top layer, ASS lower layer during compaction – notch in LM layer (inverted beam); Ph.Eur., European Pharmacopoeia; por, porosity; SSY, small scale yielding.

* Tel.: +44 020 7697 7178; fax: +44 020 7388 0180.
*E-mail addresses:* f.podczeck@ucl.ac.uk, f_podczeck@meng.ucl.ac.uk

0378-5173/$ – see front matter © 2011 Elsevier B.V. All rights reserved.
doi:10.1016/j.ijpharm.2011.02.007

**Nomenclature**

| | |
|---|---|
| $a$ | notch depth [m] |
| $b$ | beam width [m] |
| $bf$ | constant in exponential equation |
| $b_s$ | constant of Spinner's equation |
| $c_s$ | constant of Spinner's equation |
| $E$ | Young's modulus of elasticity [Pa] |
| $E_0$ | Young's modulus at zero porosity [GPa] |
| $E_{top}$ | Young's modulus of the top layer material [GPa] |
| $G$ | rigidity modulus [Pa] |
| $G_{IC}^{\infty}$ | critical strain energy release rate (far field solution) [N/m] |
| $h_{top}$ | thickness of the top layer [m] |
| $k_i$ | exponent of the Ryshkewitch equation |
| $k_m$ | constant in exponential equation |
| $K_{IC}^{I}$ | critical stress intensity factor of a compact (mode I) [Pa m$^{0.5}$] |
| $K_{IC}^{IF}$ | critical stress intensity factor of the interface (mode I) [Pa m$^{0.5}$] |
| $K_{IC}^{\infty}$ | far field stress intensity factor (mode I) [Pa m$^{0.5}$] |
| $K_{IC0}^{\infty}$ | far field stress intensity factor at zero porosity (mode I) [Pa m$^{0.5}$] |
| $L$ | tablet dimension (e.g. diameter) [m] |
| $l$ | distance between lower supports [m] |
| $l_{pl}$ | radius of the plastic zone ahead of the crack tip [m] |
| $M$ | bending moment in three-point loading [Nm] |
| $P$ | load [N] |
| $p$ | mechanical mismatch constant |
| $t$ | beam thickness [m] |
| $u_i$ | volume fraction |
| $Y$ | calibration term |
| $\Delta l$ | change in length [m] |
| $\Delta T$ | change in temperature [K] |
| $\alpha$ | thermal expansion coefficient [K$^{-1}$] |
| $\Delta\alpha$ | difference between two thermal; expansion coefficients [K$^{-1}$] |
| $\alpha_D$ | first Dundurs parameter |
| $\beta_D$ | second Dundurs parameter |
| $\nu$ | Poisson's ratio of the material |
| $\nu_{top}$ | Poisson's ratio of the top layer material |
| $\Sigma$ | stiffness ratio |
| $\sigma$ | tensile strength of a beam [MPa] |
| $\sigma_i$ | tensile strength of single powder tablet [MPa] |
| $\sigma_m$ | tensile strength of tablet made from binary powder mixture [MPa] |
| $\bar{\sigma}_m$ | tensile strength of tablet made from binary powder mixture at zero porosity [MPa] |
| $\sigma_T$ | thermal stress [Pa] |
| $\sigma_{top}$ | residual stress in the top layer [Pa] |
| $\sigma_Y$ | yield strength of the material [MPa] |
| $\Omega(\alpha_D,\lambda_0)$ | decohesion number |

adhesion. The development of various mechanical stresses during compaction and particularly during the unloading phase and tablet ejection, which could contribute to delamination, has been studied by, for example, Inman et al. (2007, 2009) and Anuar and Briscoe (2009, 2010). Podczeck and Al-Muti (2010) reported that if the material forming the lower layer of a bilayer tablet was more elastic, then the tension introduced into the system weakened the strength of the layered compacts. However, despite all these reports, the full problem of layered tablet delamination has not yet been solved, and more reasons for delamination must be identified and controlled. It is also necessary to devise an experimental method that can be used on bilayer/multilayer tablets to detect lamination tendencies that are not already obvious after tablet ejection, but only manifest themselves after storage and handling of the compacts.

The aim of this work is to explore the theoretical influence of thermal stresses and strains that can develop during tabletting and to devise an experimental method that can be used to detect delamination tendencies in bilayered tablets.

## 2. The theoretical influence of thermal stresses/strains on delamination

In this work, principles of fracture mechanics will be used to explore the delamination tendencies observed in the manufacture of bilayer tablets ("bimaterials"). Tablets are here idealised as a mathematical continuum field, which can be characterised by its elasticity and its thermodynamic behaviour. While the thermomechanical state of standard tablets can be described using a series of equations for stress and strain for a variety of loading conditions, the problem of adhesion between the layers of bimaterials is more difficult. Bimaterials can fail by various phenomena including delamination of the material layers or direct fracture within the bulk of the separate material layers. From the viewpoint of fracture mechanics, the breaking of the bulk material and the delamination of material layers are two aspects of the same phenomenon i.e. the failure of a solid body due to an excessive loading condition. Tablets are inhomogeneous porous bodies incorporating many cracks and flaws inside the bulk and along any interface with the surrounding environment and between layers. The cracks and flaws introduce stress singularities into the tablets, and the maximum stress acts at the tip of them. Bulk layers fail due to crack propagation, and equally bimaterials show delamination due to crack propagation along the interface. This process consumes energy, and it is thus important to understand where during the manufacture of bilayer tablets this energy is generated and how much is required to cause the tablets to fail.

During the process of tabletting a number of heat-generating mechanisms, e.g. interparticulate friction, particle-die wall friction, particle deformation and particle fracture occur, and as a result there is typically a more or less obvious increase in temperature and tablets often feel warm on touch after tablet ejection. Using a very slow compaction method taking a total of 17 s to achieve maximum load, dwelling, decompression and ejection, Buckner et al. (2010) reported an increase in bulk temperature up to 2.5 K for microcrystalline cellulose. However, this slow compaction process will release much less heat than compressing tablets on a high-speed tabletting machine due to the fact that all heat-generating processes mentioned above happen in "slow-motion", allowing for heat removal by conduction to the surrounding punch and die system, which provides a large heat sink. An increase in the overall temperature of tablets between 10 and 20 K during high-speed compression would seem to be a more reasonable assumption. The thermal strain created in a tablet during compression parallel to the interface can be estimated from (Hertzberg, 1996):

$$\Delta l = \alpha \Delta T L \tag{1}$$

where $\Delta l$ is the change in length; $\alpha$ is the thermal expansion coefficient of the material; $\Delta T$ is the change in temperature; and $L$ is the dimension of the tablet (e.g., diameter of a disc-shaped, or length of a capsule-shaped tablet). The thermal strain can then be calculated as % of the dimensions of the tablet. The corresponding thermal stress $\sigma_T$ is estimated from (Hertzberg, 1996):

$$\sigma_T = \frac{E\alpha\Delta T}{1-\nu} \tag{2}$$

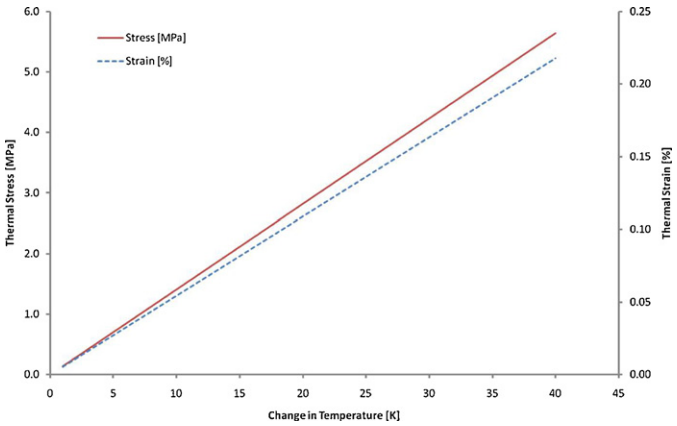


**Fig. 1.** Thermal stress and strain as a function of temperature changes during compaction, simulated for acetylsalicylic acid (ASS) compacts, for which Young's modulus, thermal expansion coefficient and Poisson's ratio are listed in Table 1.

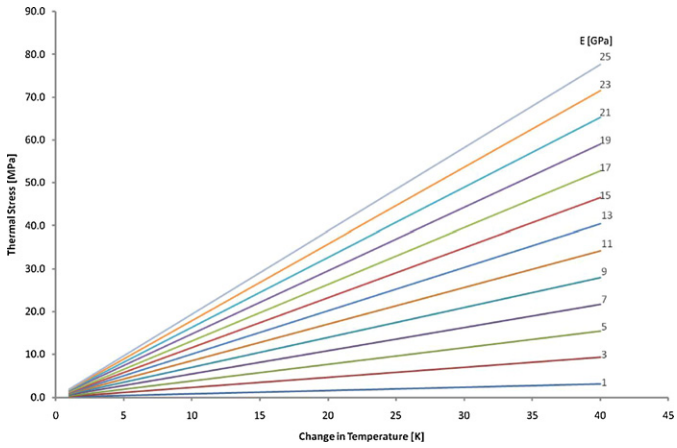


**Fig. 2.** Thermal stress as a function of temperature changes during compaction simulated for materials with a Young's modulus between 1 and 25 GPa, using the thermal expansion coefficient of ASS.

where $E$ is the Young's modulus of elasticity, and $\nu$ is Poisson's ratio of the material. The thermal stress is independent of the dimensions of the tablet. If the value of $\sigma_T$ is considerably smaller than the tensile strength of a tablet made only from this material, then the thermal stress in the bilayer tablet is not large enough to initiate delamination. However, if the thermal stress reaches or exceeds the tensile strength, then delamination will occur either during or shortly after tablet ejection i.e. during the cooling phase, or during transport and handling of the bilayer tablets. Mismatch in thermal strain between the two layers will add to the problem (Evans and Marshall, 1989), because the tablet layers are made to the same dimensions during compression and the surfaces are welded together. Different thermal strain will force the layers into different degrees of expansion, which can only happen if the adhesion between the layers is reduced, leading to crack formation and delamination, especially at the layer interface at the tablet circumference.

In Fig. 1 thermal stress and strain are simulated as a function of temperature change during compaction for acetylsalicylic acid (ASS) compacts, for which Young's modulus, thermal expansion coefficient and Poisson's ratio are listed in Table 1. This model drug is very elastic, and its value for the Young's modulus is at the lower end of the values for active pharmaceutical ingredients (APIs) and excipients. Rowe and Robert (1995) reported Young's modulus values as large as 45 GPa (sorbitol instant), for various lactose forms between 11 and 24 GPa, and for microcrystalline cellulose brands between 7 and 10 GPa. All values for APIs that these authors reported were well above that of ASS. In Fig. 2 the thermal stresses are hence simulated for materials with a Young's modulus between 1 and 25 GPa, using the thermal expansion coefficient of ASS as an example to be able to compare the effects studied in Figs. 1 and 2. It can be seen that stiffer materials produce large thermal stresses well above the typical tensile strength of tablets (2–3 MPa), and delamination is hence likely. The comparison of the two figures implies that an elastic mismatch appears to be more destructive to a layered tablet than the thermal stresses due to heat development.

Having explored the influence of thermal stresses on the individual materials of a potential bilayer tablet, it is now interesting to see the effects of these stresses on a model bimaterial made from

**Table 1**
Mechanical and physical data for acetylsalicylic acid (ASS) and lactose monohydrate (LM).

| Parameter | Symbol [units] | ASS | LM |
|---|---|---|---|
| Young's modulus | $E$ [GPa] | $1.84 \pm 0.03$[a] | $2.99 \pm 0.06$[a] |
| Rigidity modulus[b] | $G$ [GPa] | 0.71 | 1.25 |
| Poisson's ratio | $\nu$ | 0.29[c] | 0.20[d] |
| Yield strength | $\sigma_Y$ [MPa] | $36.7 \pm 1.7$[a] | $91.6 \pm 9.4$[a] |
| Critical stress intensity factors | | | |
| Mode I | $K^I_{IC0}$ [kPa m$^{0.5}$] | $366 \pm 12$[a] | $493 \pm 32$[a] |
| Mode II | $K^{II}_{IC0}$ [kPa m$^{0.5}$] | $895 \pm 85$[e] | $771 \pm 127$[e] |
| Mode III | $K^{III}_{IC0}$ [MPa m$^{0.5}$] | $>15.1 \pm 0.8$[f] | $102 \pm 14$[f] |
| Critical strain energy release rate | | | |
| Mode I | $G^I_{IC}$ [Nm$^{-1}$] | 66.2[a] | 74.0[a] |
| Plastic component of fracture toughness | | | |
| Mode I | $J^p_{IC}$ [Nm$^{-1}$] | $5.9 \pm 0.3$[a] | $8.7 \pm 0.8$[a] |
| Shear fracture stress | $\tau_f$ [kPa] | $0.63 \pm 0.08$[e] | $1.20 \pm 0.13$[e] |
| $K^I_{IC}/K^{II}_{IC}$ | | 0.41[e] | 0.64[e] |
| Thermal expansion coefficient | $\alpha$ [K$^{-1}$] | $54.4 \times 10^{-6}$ [g] | $28.6 \times 10^{-6}$[h] |
| Zero tensile strength | $\sigma_0$ [MPa] | $9.8 \pm 0.2$[a] | $33.0 \pm 1.5$[a] |

[a] Podczeck (2001a).
[b] Calculated according to Roark (2002) as $G = E/(2(1+\nu))$.
[c] Roberts et al. (1994).
[d] Hassanpour et al. (2003).
[e] Podczeck (2002).
[f] Podczeck (2001b).
[g] Bauer et al. (2010) (average of single crystal dimension data).
[h] Derived from specific heat reported by Buckner et al. (2010).

an API i.e. here ASS and a commonly used excipient i.e. here lactose monohydrate (LM). The mechanical properties of these materials are summarised in Table 1. The differences in the mechanical properties will cause a mechanical mismatch and potentially a steady state cracking along the interface between the two layers, especially when thermal stresses are assumed due to the warming of the compact during tabletting. At the interface in steady-state the critical stress intensity factors in modes II and III (crack sliding and crack tearing, respectively) are zero, because crack propagation is solely the result of crack opening. The critical stress intensity factor of the interface in mode I (tensile failure of the interface, $K_{IC}^{IF}$) is defined as (Lacombe, 2006):

$$K_{IC}^{IF} = \sigma_{top}\sqrt{h_{top}}\Omega(\alpha_D, \lambda_0) \quad (3)$$

where $\sigma_{top}$ is the residual stress in the top layer after tabletting, $h_{top}$ is the thickness of the top layer, and $\Omega(\alpha_D, \lambda_0)$ is called the decohesion number. The decohesion number has been defined and tabulated by Suo and Hutchinson (1990) and is based on the work by Dundurs (1969), who first explored the effect of elastic dissimilarities within layered materials. Suo and Hutchinson (1990) provided a set of fitted equations to estimate the decohesion number as follows:

$$\Omega(\alpha_D, \lambda_0) = (3.5\Sigma - 0.63)^{0.5} \quad 1 \le \Sigma \le 10 \quad (4)$$

$$\Omega(\alpha_D, \lambda_0) = (0.944\Sigma^{-0.4} - 0.63) \quad 0.1 \le \Sigma \le 1 \quad (5)$$

where $\Sigma$ is the stiffness ratio defined by Dundurs (1969):

$$\Sigma = \frac{c_1}{c_2} \quad (6)$$

Under in plane-strain conditions i.e. typical test conditions for tablets whereby the tablets are strained and the resulting stress is recorded, the terms $c_1$ and $c_2$ are determined from the Poisson's ratio $\nu$ and the rigidity modulus $G$ of the two materials forming the bimaterial:

$$c_i = \frac{(3 - 4\nu_i + 1)}{G_i} \quad (i = 1, 2) \quad (7)$$

Assuming a bilayer tablet made from ASS and LM, the stiffness ratio $\Sigma$ will depend on which material forms the top and which one the lower layer i.e. using the material data listed in Table 1, the stiffness ratio would be 1.56 and 0.64 for ASS forming the top or the lower layer, respectively. This results in decohesion numbers of 2.2 and 0.5. The residual stress in the top layer of the bimaterials is calculated using a modification of Eq. (2), i.e.:

$$\sigma_{top} = \frac{E\Delta\alpha\Delta T}{1 - \nu} \quad (8)$$

With an estimated difference between the thermal expansion coefficients (see Table 1) of the two materials of $\Delta\alpha = 26 \times 10^{-6}\,K^{-1}$ and an estimated increase in temperature during tabletting of 20 K this results in top layer residual stresses of 1.35 MPa and 1.94 MPa for ASS and LM, respectively. These stresses are quite high indicating a tendency to crack formation along the interface and potential delamination. Assuming a layer thickness of $h_{top} = 3$ mm, the critical stress intensity factor of the interface can be calculated (Eq. (3)) to be 160 kPa $m^{0.5}$ and 53 kPa $m^{0.5}$ for ASS and LM forming the top layer of the bimaterial, respectively. These are the critical values to be reached for steady-state crack propagation i.e. delamination to commence.

## 3. Experimental procedure to detect delamination tendencies

The above outlined theoretical considerations could explain why in certain instances laminated tablets will delaminate shortly after manufacture or during handling and storage. However, unless the delamination starts directly after the tabletting process and prior to packaging, it will still require regular inspection to identify delaminating tablet batches. This is tedious and once the tablets have been distributed to the end user, more or less impossible. It is hence necessary to identify a test procedure that can detect delamination tendencies and can be used as quality control procedure. As the above theories are routed in fracture mechanics, it appears sensible to use a fracture mechanics test procedure to identify whether during the manufacture, either due to thermal stresses or mechanical mismatch between the layers, microscopic cracks have formed at the layer interface that can propagate when the tablets are handled.

Three-point bending of beams is frequently used in mechanical testing of brittle specimens (Stanley, 2001) and it is hence not surprising that it is also the method of choice when working with bimaterials (Evans et al., 1989, 1990; Zhang et al., 2004). The critical stress intensity factor in mode I for solid beams of pharmaceutical materials as reported by many workers such as Mashadi and Newton (1987), York et al. (1990) and Podczeck (2001a) determines the stress developing at the tip of a preformed crack that is required to propagate this crack so that the beam fails in tension. For this to happen under controlled conditions a notch is inserted in the middle of the lower side of the beam. A similar approach can be used to determine whether there are cracks along the interface that could propagate. However, in contrast to the critical stress intensity factor determined on single material beams, here a far field solution has to be used i.e. the tip of the crack is at a defined distance away from the interface, which the calculations must take into account. The critical stress intensity factor of the specimen $K_{IC}^{I}$ is related to the far field stress intensity factor $K_{IC}^{\infty}$ via a constant $p$ ($K_{IC}^{I} = p \times K_{IC}^{\infty}$), which reflects the mismatch in the mechanical properties of the layer materials (Suo and Hutchinson, 1990):

$$p = \sqrt{\frac{1 - \alpha_D}{1 - \beta_D^2}} \quad (9)$$

where $\alpha$ and $\beta$ are the Dundurs parameters (Dundurs, 1969), defined as follows:

$$\alpha_D = \frac{\Gamma(\kappa_2 + 1) - (\kappa_1 + 1)}{\Gamma(\kappa_2 + 1) + (\kappa_1 + 1)} \quad (10)$$

$$\beta_D = \frac{\Gamma(\kappa_2 - 1) - (\kappa_1 - 1)}{\Gamma(\kappa_2 + 1) + (\kappa_1 + 1)} \quad (11)$$

$$\Gamma = \frac{G_1}{G_2} \quad (12)$$

$$\kappa_i = 3 - 4\nu_i \quad (i = 1, 2) \quad (13)$$

where $G_i$ ($i = 1, 2$) is the rigidity modulus of the materials forming the layers, and $\nu_i$ ($i = 1, 2$) is as before the Poisson's ratio of the materials. Eq. (13) is valid for plane-strain conditions only.

The critical stress intensity factor of the specimen in mode I, $K_{IC}^{I}$, is determined experimentally following the method described by Brown and Srawley (1967):

$$K_{IC}^{I} = Y\frac{6Ma^{0.5}}{bt^2} \quad (14)$$

$$M = \frac{Pl}{4} \quad (15)$$

where $M$ is the bending moment in three-point loading, $a$ is the depth of the notch (see Fig. 3), $b$ is the width of the beam, $t$ is the thickness of the beam, $P$ is the load applied to cause the beam to fail in tension, $l$ is the distance between the lower supports (see Fig. 3), and $Y$ is a calibration term (Gross and Srawley, 1965):

$$Y = C_0 + C_1\left(\frac{a}{t}\right) + C_2\left(\frac{a}{t}\right)^2 + C_3\left(\frac{a}{t}\right)^3 + C_4\left(\frac{a}{t}\right)^4 \quad (16)$$

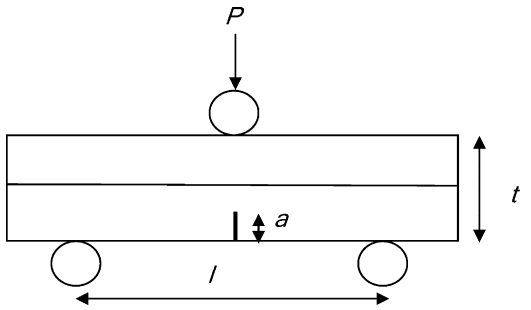


**Fig. 3.** Schematic illustration of the three-point bending test of notched bimaterials. A beam of thickness $t$ rests on two lower support rolls which are a defined distance apart ($l$), and a similar roll is used to load the system until it fails in tension ($P$). The notch ($a$) is at the lower surface of the beam directly underneath the upper loading roll. The notch tip is not in close proximity or contact with the interface.

where the coefficients $C_i$ ($i = 0, \ldots, 4$) have been determined by Podczeck (1997):

$$C_0 = \frac{7.5 \times 10^{-3} l}{t} + 1.90 \quad (17.0)$$

$$C_1 = \frac{8.0 \times 10^{-2} l}{t} - 3.39 \quad (17.1)$$

$$C_2 = \frac{-0.2175 l}{t} + 15.40 \quad (17.2)$$

$$C_3 = \frac{0.2825 l}{t} - 26.24 \quad (17.3)$$

$$C_4 = \frac{0.1450 l}{t} + 26.38 \quad (17.4)$$

The value of $K_{IC}^{\infty}$ is then determined as described above using the value of $p$ (Eq. (9)). The critical strain energy release rate of the interface $G_{IC}^{\infty}$ (far field solution) can then be calculated from (Phillipps et al., 1993):

$$G_{IC}^{\infty} = \frac{(K_{IC}^{\infty})^2}{E'} \quad (18)$$

$$E' = \frac{(E_{top})}{(1 - \nu_{top})} \quad (19)$$

where $E'$ is determined solely by the Young's modulus and the Poisson's ratio of the unnotched (i.e. top) layer.

Composite theory would predict that the critical stress intensity factor of the bimaterials without tendency to delaminate should exceed the values of the individual materials used to form the layers. Hence, lamination tendencies can first of all be identified by comparing the $K_{IC}^{I}$ values of each layer material with the $K_{IC}^{\infty}$ value determined (Chen et al., 2007). If the latter is significantly smaller than the values for the individual materials, the interface was weakened by small cracks and the bimaterial would eventually delaminate. Evans and Marshall (1989) defined a critical value for delamination as the ratio between the critical strain energy release rates of interface and top layer material of less or just equal to 0.25. However, they could not provide a direct experimental validation for this requirement. A further comparison can be made between the predicted values for the critical stress intensity factor of the interface (Eq. (3)) and the experimental values for the far field stress intensity factor, using different top layers. If the experimental values do not reach or exceed the predicted values, then delamination will not readily occur (see above). However, values similar or larger than the predicted values indicate that the interface has been weakened by cracks and delamination might result during handling of these specimens.

## 4. Materials and methods

### 4.1. Materials

The following powders (Ph.Eur. quality) were used: acetylsalicylic acid (ASS; Rütgers Organics GmbH, CF Aubing Pharmaceutical, Mannheim, Germany, batch 98070230), lactose monohydrate (LM; Borculo Whey Products, Saltney, UK, batch 826704).

### 4.2. Particle size analysis

The particle size was determined using light microscopy (Olympus BH–2, Tokyo, Japan) in connection with image analysis (Seescan Solitaire 512, Cambridge, UK). One thousand particles were inspected, and the mean Feret diameter was determined to be $8.8 \pm 4.8$ μm and $6.1 \pm 3.9$ μm for ASS and LM, respectively.

### 4.3. Particle density

The particle density was determined with an air pycnometer (Model 930, Beckman Instruments Inc., USA) and is $1400 \pm 2$ kg m$^{-3}$ and $1540 \pm 1$ kg m$^{-3}$ for ASS and LM, respectively (arithmetic mean and standard deviation of 5 replicates).

### 4.4. Powder mixing

For the preparation of mixed beams, powder mixtures in a ratio of 1:1 (v/v) ASS to LM were produced i.e. 71.43 g ASS and 78.57 g LM were mixed in a 250 ml brown glass jar using a tumbler mixer (Willy A. Bachofen AG Maschinenfabrik, Basel, Switzerland) for 30 min at a mixing speed of 42 rpm. Three mixtures were prepared, and the homogeneity of each mixture was determined by sampling two samples from the surface, one from the centre and two from the bottom of the mixing vessel using a Micro Mate® low volume powder sampler (Sampling Systems Ltd., Coleshill, Warwickshire, UK). Each sample was accurately weighed to a precision of ±0.0001 g (electronic recording balance, Sartorius AG Göttingen, Germany), dissolved in ethanol (BDH, Poole, UK), and the ASS concentration was determined by UV spectrophotometry ($\lambda = 278$ nm; Cecil CE2020, Cecil Instruments, Cambridge, UK). The relative standard deviation of the drug content ranged between 2.95 and 3.15% indicating that sufficient mixing homogeneity had been achieved.

### 4.5. Manufacture of beams

The compacted powder specimens were prepared using a specially manufactured split-die system made from hardened stainless steel. All parts of this system were polished after each compaction to avoid the use of lubricant, as the latter could potentially contaminate the interface between the tablet layers and hence add to delamination by reduction of interfacial adhesion forces. The nominal dimensions of the die were $45 \times 9$ mm and the target thickness of each layered compact was 5 mm immediately after ejection from the die. The split-die could be completely dismantled to allow removal of the compact specimen without exerting an ejection force. The compaction force was applied using a hydraulic press (Specac 15,000, Specac Ltd., Kent, UK). A summary of the target beam porosities, compaction pressures, and weights of individual layers and final beams is given in Table 2.

For each experimental series 34 layered beams were produced, and four experimental series were run i.e. two series with ASS as top and LM as lower layer, and two series with LM as top and ASS as lower layer during compression. For reference, beams from a 1:1 (v/v) powder mixture (see above) were also produced, and the quantities used for these beams are identical to those listed in Table 2, column "total weight". For each test series 34 beams were

**Table 2**
Summary of the target beam porosity values, compaction pressures, and weights of individual layers and final beams used in all four series of experiments. The differences in weight for ASS and LM result from the different particle densities, as all calculations were aimed at achieving similar volume. In each series, all porosity values listed were replicated twice to give a total number of beams per series of 34.

| Porosity | Pressure [MPa] | Total weight [g] | ASS weight [g] | LM weight [g] |
|---|---|---|---|---|
| 0.20 | 12.1 | 2.381 | 1.134 | 1.247 |
| 0.19 | 18.2 | 2.411 | 1.148 | 1.263 |
| 0.18 | 24.2 | 2.441 | 1.162 | 1.279 |
| 0.17 | 31.5 | 2.471 | 1.177 | 1.294 |
| 0.16 | 38.8 | 2.500 | 1.190 | 1.310 |
| 0.15 | 48.4 | 2.530 | 1.205 | 1.325 |
| 0.14 | 60.6 | 2.560 | 1.219 | 1.341 |
| 0.13 | 75.1 | 2.590 | 1.233 | 1.357 |
| 0.12 | 87.2 | 2.620 | 1.248 | 1.372 |
| 0.11 | 102.9 | 2.649 | 1.261 | 1.388 |
| 0.10 | 121.1 | 2.679 | 1.276 | 1.403 |
| 0.09 | 139.3 | 2.709 | 1.290 | 1.419 |
| 0.08 | 157.4 | 2.739 | 1.304 | 1.435 |
| 0.07 | 175.6 | 2.768 | 1.318 | 1.450 |
| 0.06 | 199.8 | 2.798 | 1.332 | 1.466 |
| 0.05 | 230.1 | 2.828 | 1.347 | 1.481 |
| 0.04 | 266.4 | 2.858 | 1.361 | 1.497 |

produced, and two series were prepared. In addition, a third series of 34 mixed powder beams was produced with all beams having a target porosity of 0.20.

The quantities required to make each type of beams were weighed to a precision of ±0.0001 g (electronic recording balance, Sartorius AG Göttingen, Germany). The weighed powder quantities for the lower beam layer were transferred to the punch assembly, carefully levelled using a spatula and the upper punch was placed on the lower powder bed for 10 s to produce an even and stable surface prior to the addition of the powder required for the upper layer. After careful levelling of the upper powder layer, the beams were compressed using the full calculated target pressure and a dwell time of 5 s. To have achieved the target thickness of the beams was confirmed using a digital micrometer (electronic callipers, Moore & Wright, Sheffield, UK) with a precision of ±0.001 mm. The upper surface of each beam was marked immediately after removal from the die using a soft pencil. All compacts were stored under controlled humidity of 53% at 20 °C for two weeks using large desiccators filled with saturated solutions of magnesium nitrate (BDH, Poole, UK) and then tested.

### 4.6. Determination of beam and layer dimensions

After storage of the beams for two weeks to allow for relaxation, the length of each compact was measured using electronic callipers (Moore & Wright, Sheffield, UK) to an accuracy of ±0.01 mm. The compact width was measured to an accuracy of ±0.001 mm at three positions along the compact (i.e. left and right edge plus middle) using digital callipers (Moore & Wright, Sheffield, UK), and the mean width value was calculated.

A computerised image analysis system (Solitaire 512, Seescan, Cambridge, UK) connected to a black and white camera (CCD-4 miniature video camera module, Rengo Co. Ltd., Toyohashi, Japan), zoom lens (18–108/2.5, Olympus Europe, Hamburg, Germany) and cold light source (Olympus highlight 3000, Olympus Europe, Hamburg, Germany) was used to determine the thickness of each layer contributing to the layered compacts. The image analysis measurements were taken assuming a standard imaging error of ±1 pixel, which was calibrated each day, and which ranged between ±35.75 μm and ±35.53 μm. Adjustments to the recorded layer thickness have been made based on the pixel errors to account for the difficulties in accurate determination of the exact boundary between the separate layers and also between the solid materials and air.

### 4.7. Porosity of beams and beam layers

The porosity of the beams and beam layers was determined from the dimensions of the beams/beam layers after storage, the beam weight and powder weight used for individual layers, and the particle density.

### 4.8. Production of notched specimen

For the determination of the far field stress intensity factor, a sharp notch has to be introduced into the surface that will face downwards during the three-point bending test (see Fig. 3). A Japanese pull saw was used, which produced sharp notches of 100 μm in width. The required target depth of the notches for stable and controlled crack propagation was assumed to be similar to those used earlier to determine the critical stress intensity factor in Mode I on solid beams (Podczeck, 2001a) i.e. 800 μm and 600 μm for ASS and LM, respectively. The notches were measured on both sides using a microscope (Olympus BH–2, Tokyo, Japan) attached to the image analyser (see above). The magnification was chosen so that the standard imaging error of 1 pixel resulted in a measuring error of 5.714 μm. The average notch depth was used in the calculations.

### 4.9. Determination of the breaking load

Three-point bending experiments (see Fig. 3) were performed in order to determine the breaking load of the compacts using a universal strength tester (CT-5, Engineering Systems, Nottingham, UK) set at a test speed of 1 mm $min^{-1}$, and using a 5 kg load cell (Engineering Systems, Nottingham, UK). The three-point bending rig attached to the system was set at a span width of 36 mm. The force reading was taken from the digital output of the CT–5, and fracture load data as a function of time were recorded as a chart (recording speed 200 mm/min; Venture x-t plotter, Servoscribe, UK) to determine potential crack arrest at the interface between the compact layers.

### 4.10. Data processing and statistical analysis

All calculations were undertaken using Microsoft Excel 2007, and all statistical analysis was carried out using SPSS 17.0 (SPSS Inc., Woking, UK). Non-linear relationships were always treated with non-linear regression analysis to minimise errors when obtaining extrapolations to zero porosity.

## 5. Results and discussion

### 5.1. Binary powder mixture beams

Wu and Seville (2009) compared the compaction properties of binary and bilayer tablets with the aim to understand the contribution of each individual material to the strength of the different systems. In this work, hence, a similar strategy has been chosen. In a first step, the basic mechanical parameters such as Young's modulus of elasticity, yield strength and critical stress intensity factor (mode I) were determined.

"At zero pressure" Heckel analysis (Heckel, 1961a,b) was performed i.e. the relative density of the specimens after complete relaxation of the beams during storage was used in the calculations. This ensures that the Heckel constants are not affected by elastic deformation that occurs during compaction. The Heckel plot was linear above a compaction pressure of 150 MPa ($R^2$ = 0.997,

RMS = 0.34%). The resulting yield strength for the binary powder mixture is 87.5 ± 0.1 MPa. This value is relatively similar to that previously found for LM (see Table 1), indicating that the yield strength of the powder mixture is predominantly reflecting the properties of the excipient.

The Young's modulus was obtained from unnotched beams by determining the breaking load and the beam deflection at the midpoint under load, as described previously (Podczeck, 2001a). The values for each individual beam and their porosity were used to determine the Young's modulus at zero porosity $E_0$ by fitting the data to Spinner's equation (Spinner et al., 1963):

$$E = E_0(1 - b_s \times por - c_s \times por^2) \quad (20)$$

where $E$ is the Young's modulus of the individual beam, *por* is the porosity of the beam, and $b_s$ and $c_s$ are constants. The value for $E_0$ was found to be 1.99 ± 0.06 GPa ($R^2$ = 0.975, RMS = 2.02%). In contrast to the yield strength, this value is very similar to the Young's modulus of ASS (see Table 1) i.e. while the ability of the mixed beams to deform permanently appears to be governed by LM, the reversible deformation depends here on the incorporated ASS. However, the bi-exponential behaviour of ASS alone, as reported previously (Podczeck, 2001a), is not present, indicating that LM disturbs the equilibrium between structural faults within and at the surface of the beams during compaction and the amount of particle surfaces welding together by bond formation appears to exceed the amount of new surfaces formed due to fragmentation during compaction.

All beams used for the determination of the Young's modulus of the powder mixture failed catastrophically and in tension. Hence, the tensile strength of each beam was determined as described by Stanley (2001) and the tensile strength at zero porosity was extrapolated using an exponential function (Ryshkewitch, 1953; Duckworth, 1953). With an extrapolated value of 13.4 ± 0.6 MPa ($R^2$ = 0.961, RMS = 2.8%) again this parameter of mechanical strength is more related to ASS than LM (see Table 1).

The experimental value of $K_{IC}^I$ depends on the depth of the crack length introduced into the beam (see Fig. 3) to control crack propagation. Initially, the value increases with an increase in notch depth. However, eventually a limiting notch depth is reached, above which the value for $K_{IC}^I$ becomes constant and independent of notch depth (Brown and Srawley, 1967). For the determination of the critical stress intensity factor at zero porosity it is hence necessary to determine the $K_{IC}^I$ using beams with a notch depth above the limiting value. For ASS and LM the minimum notch depth had previously been found to be 620 μm and 400 μm, respectively (Podczeck, 2001a). Similar to the previous work, the minimum notch depth for mixed beams was determined using beams with a porosity of 20% (see Fig. 4a). A minimum value of 850 μm was found, indicating that the fracture mechanics and consequently the strength of the mixed beams are somewhat different from the beams made from the individual materials. For the determination of the critical stress intensity factor at zero porosity beams with porosity values varying between 20% and 5% were used (see Fig. 4b), and a target notch size of 1 mm was employed. The average notch size achieved was 1125 ± 130 μm. The extrapolated critical stress intensity factor at zero porosity is 395.7 ± 9.9 kPa m$^{0.5}$ ($R^2$ = 0.983, RMS = 1.99%). While significantly different from the value reported for ASS (see Table 1), this value is much closer to ASS than to LM, indicating that ASS dominates the behaviour of the mixed beams. As described in Podczeck (2001a) it is possible to determine the length of the cracks and flaws inside the beams from the results shown in Fig. 4b and the corresponding values for Young's modulus and tensile strength of beams of similar porosity and composition (data not shown, but used above for the determination of $E_0$). The average crack length inherent in the mixed beams is 214 μm (95% confidence interval: 109–319 μm, $R^2$ = 0.976, RMS = 12.0%). Hence, considering the size

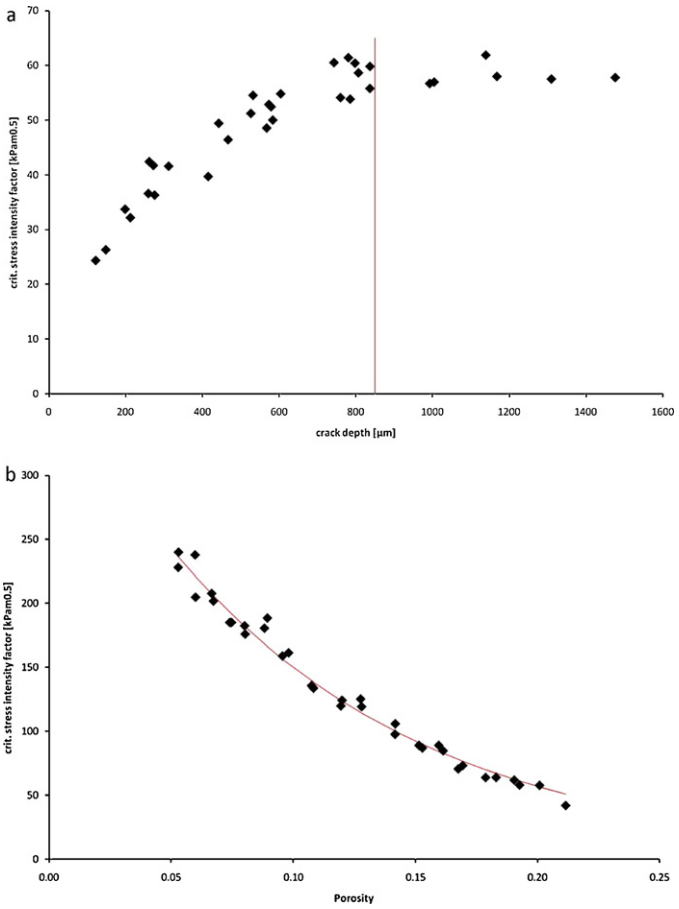


**Fig. 4.** Determination of the critical stress intensity factor in mode I loading using mixed beams (ASS:LM = 1:1 (v/v)). (a) Determination of the critical crack length; (b) exponential relationship between the critical stress intensity factor and beam porosity.

of the individual particles of the two materials, compacts made from a mixture of 1:1 (v/v) ASS and LM have cracks and flaws, which are proceeding along particle boundaries linking pores along several particles. Crack propagation will hence most likely follow particle boundaries. The large flaw size is also an indication that the adhesion forces between ASS and LM particles are smaller and welding of their surfaces is less favoured than welding between particles of the same material. Hence there might be a tendency for delamination in bimaterials made from these two powders. Wu et al. (2005) reported that it should be possible to predict the strength of tablets made from binary powder mixtures from the tensile strength of tablets made from the individual components using the following relationship:

$$\sigma_m = \bar{\sigma}_m e^{-k_m(por)} \quad (21)$$

where $\sigma_m$ is the tensile strength of a binary tablet, *por* is the tablet porosity, $k_m = \sum k_i u_i (i = 1, 2)$, and $\bar{\sigma}_m = \sum \sigma_i u_i (i = 1, 2)$ with $k_i$, $\sigma_i$ and $u_i$ being the exponential constant of the Ryshkewitch equation (Ryshkewitch, 1953), tensile strength and volume fraction of tablets made from the individual materials, respectively. For zero porosity, $\sigma_m$ should be equal to $\bar{\sigma}_m$. However, calculating the value for $\bar{\sigma}_m$ using the tensile strength values provided in Table 1 arrives at 21.4 MPa, which is much larger than the experimental value of 13.4 MPa (see above). This discrepancy points either to limited adhesion between the ASS and LM particles in mixed compacts and thus a potential for delamination of equivalent bimaterials, or the equation published by Wu et al. (2005) is not applicable to these

**Table 3**
Fracture data obtained from layered beams.

| Parameter | ASS(t)/LM(c)[a] | ASS(t,c)/LM[b] | LM(t)/ASS(c)[c] | LM(t,c)/ASS[d] |
|---|---|---|---|---|
| $K_{IC0}^{\infty}$ [kPa m$^{0.5}$] | | | | |
| BP[e] | 175.5 ± 11.1 | 498.9 ± 38.3 | 428.1 ± 22.6 | 186.9 ± 7.8 |
| LLP[f] | 172.9 ± 13.7 | 453.6 ± 31.2 | 450.1 ± 35.5 | 171.3 ± 13.2 |
| Constant $b$[g] | | | | |
| BP | 7.285 ± 0.521 | 8.876 ± 0.503 | 9.423 ± 0.463 | 9.173 ± 0.362 |
| LLP | 5.185 ± 0.466 | 7.851 ± 0.406 | 8.380 ± 0.582 | 6.506 ± 0.506 |
| $R^2$ (RMS)[h] | | | | |
| BP | 0.887 (7.88%) | 0.931 (11.2%) | 0.950 (12.5%) | 0.965 (4.3%) |
| LLP | 0.819 (9.95%) | 0.937 (11.3%) | 0.892 (18.2%) | 0.862 (8.5%) |
| Stress type | SSY[i] | SSY | SSY | SSY |
| Crack arrest[j] | Yes | No | No | Yes |
| Radius[k] $l_{pl}$ | 30–400 nm | 1–15 μm | 1–20 μm | 20–320 nm |
| $G_{IC}^{\infty}$ [N/m] | 11.88 | 66.59 | 49.03 | 13.48 |

[a] Top layer: ASS, crack in LM layer.
[b] Top layer: ASS, crack in ASS layer ("inverted beam").
[c] Top layer: LM, crack in ASS layer.
[d] Top layer: LM, crack in LM layer ("inverted beam").
[e] Overall porosity of the beam.
[f] Porosity of the lower layer.
[g] Extrapolated far field stress intensity factor at zero porosity ($K_{IC}^{\infty} = K_{IC0}^{\infty} \times e^{-bf \times por}$).
[h] Non-linear determinant (Root Mean Square deviation of the residuals).
[i] Small scale yielding limit applies.
[j] Crack arrest at the interface between the two layers.
[k] Radius of the plastic zone ahead of the crack tip.

two materials, or to beam bending in contrast to the diametral compression of cylindrical tablets used by Wu et al. (2005).

### 5.2. Far field stress intensity factor for bimaterials

In line with previous findings (Podczeck, 2001a), for the determination of the critical stress intensity factor in mode I loading, a 600 μm crack was used in LM layers and a 800 μm crack was used in ASS layers. The process of uniaxial compression used to prepare the laminated beams resulted in different thicknesses of top and lower layer due to incomplete force transmission due to die wall and interparticulate friction. At lower compaction pressures the lower layer thickness exceeded that of the top layer. While low top layer porosity was achieved already at lower compaction pressures, the porosity of the lower layer changed more gradually with increasing compaction pressure, eventually reaching values similar to the top layer at the highest compaction pressures used. Therefore, the proposed test procedure might be affected by the differences in porosity, and hence four sets of beams were produced and tested with the crack facing downward (see Fig. 3):

1. ASS as top layer and LM as lower layer during compaction; introduction of a 600 μm crack into the LM layer ("ASS(t)/LM(c)").
2. ASS as top layer and LM as lower layer during compaction; introduction of a 800 μm crack into the ASS layer ("inverted beam"; "ASS(t,c)/LM").
3. LM as top layer and ASS as lower layer during compaction; introduction of a 800 μm crack into the ASS layer ("LM(t)/ASS(c)").
4. LM as top layer and ASS as lower layer during compaction; introduction of a 600 μm crack into the LM layer ("inverted beam"; "LM(t,c)/ASS").

After crack introduction, prior to the bending test, the beams were inspected for signs of delamination, especially at their edges, and beams for which visual evidence of delamination was found were discarded. Typically, two or three beams per test series had to be discarded, whereby these were found to have been produced with the higher compaction pressures.

For each beam the critical stress intensity factor was calculated (Eqs. (14)–(17)), and the far field stress intensity factor was determined by multiplying this value with the mechanical mismatch constant $p$ (Eqs. (9)–(13)), whereby the values for $p$ were 0.884 and 0.733 for ASS and LM forming the top layer of the bimaterials, respectively. The far field stress intensity factor at zero porosity, $K_{IC0}^{\infty}$, was then extrapolated using a simple exponential relationship ($K_{IC}^{\infty} = K_{IC0}^{\infty} \times e^{-bf \times por}$). However, the literature does not provide an answer as to whether the porosity used in this relationship should be that of the lower (i.e. downward facing) layer only, or whether it should be the overall beam porosity. This is simply, because delamination studies are typically performed on bimaterials from metal alloys, wood, polymers, etc. i.e. the specimens are non-porous. For the use of the porosity of the lower layer speaks the fact that the crack that is propagated under the controlled test conditions is introduced into the lower, downward facing layer. However, the beam will only fail if the energy released is large enough for the crack to propagate through the top layer as well, i.e. the properties of the top layer will largely influence the outcome of the bending test. Hence the use of the overall beam porosity is also justified. Therefore, the calculations were performed in comparison, using both the porosity of the lower, downward facing layer and the overall beam porosity. The results are listed in Table 3. The results using different porosity values are only marginally different. It is hence a question of how accurately the thickness of the individual layers can be determined. The use of the simpler and more accurate values for the overall beam porosity is justified by these findings.

Fig. 5 compares the far field stress intensity factors as a function of porosity of the lower, downward facing layer (Fig. 5a) and the overall beam porosity (Fig. 5b). In both Figures, there are two sets of relationships, which are a result of using either ASS or LM as the downward facing, cracked layer during the bending test. If the crack was introduced into the LM layer, then the relationship between the values of $K_{IC}^{\infty}$ and the corresponding porosity is shallow, whereas if the crack was introduced into the ASS layer, the relationship is much steeper, indicating more resistance to crack propagation and larger energy release, once the critical crack length has been reached. Those two series, where the ASS layer formed the upper layer during compaction are stronger than the comparable beams with LM forming the upper layer during compaction, independent of whether the beams were inverted for crack introduction or not.

Before the results of the bending tests can be interpreted further, it has to be ensured that a fracture mechanics approach is indeed

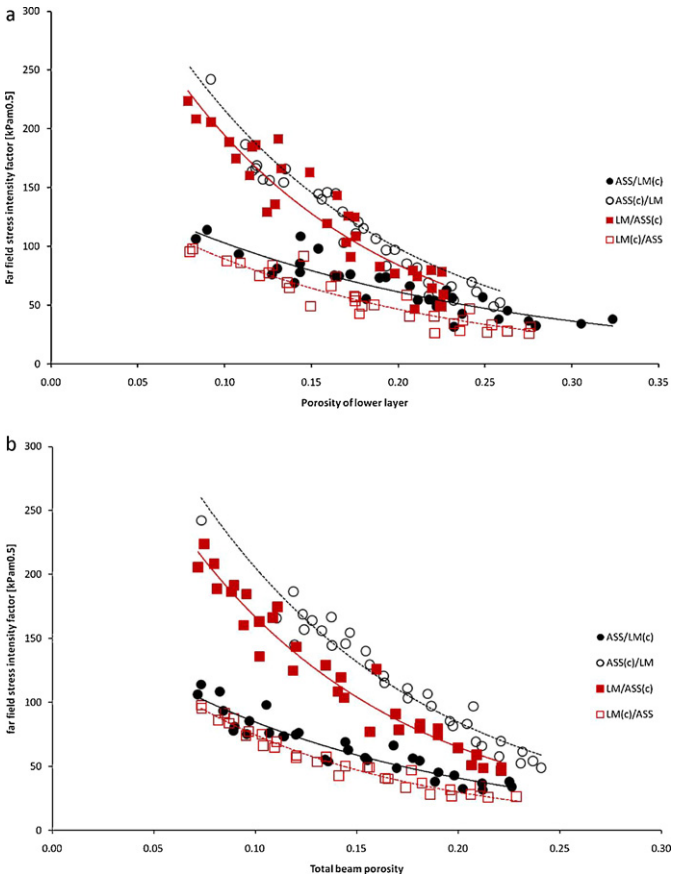


**Fig. 5.** Far field stress intensity factor as a function of porosity. (a) Porosity of the lower, downward facing notched layer; (b) overall beam porosity.

applicable. Ahead of the tip of the propagating crack the local stress introduced will typically exceed the yield strength of the material, resulting in plastic flow. The radius of this region must be negligibly small so that the local yielding can be ignored i.e. the so-called "small scale yielding" (SSY) assumption must be proven to hold (Lacombe, 2006). According to Cao and Evans (1991), the SSY limit applies if both $l_{pl}/a < 1$ and $\sigma/\sigma_Y < 1$, where $l_{pl}$ is the radius of the plastic zone ahead of the crack tip, $a$ is the notch depth, $\sigma$ is the tensile strength of the beam, and $\sigma_Y$ is the yield strength of the material. The value of $l_{pl}/a$ can be calculated from:

$$\frac{l_{pl}}{a} = 0.817\left(\frac{\sigma}{\sigma_Y}\right)^2 \quad (22)$$

For all four test series the assumption of the validity of the SSY assumption was confirmed. Therefore, the radius of the plastic zone, $l_{pl}$, was calculated by rearranging Eq. (22) and is listed in Table 3. According to Adams (1985) brittle materials have $l_{pl}$ values in the nanometre range, whereas ductile materials have $l_{pl}$ values in the micrometer range. The results hence indicate that under the stated test conditions, LM behaved as a brittle material, whereas ASS demonstrated ductility. There will hence be considerable differences in the far field stress intensity factor values, depending on whether LM or ASS are used as the downward facing layer in the experiments.

In the case that the layers are sufficiently thick i.e. considerably thicker than the propagating crack (with a notch depth of significantly less than 1 mm and a layer thickness between 2 and 3 mm this applies here), the failure of the bilayer tablets will be flaw controlled and is hence related to the tensile strength of the individual materials (He et al., 1993). Hence, when the crack propagates from the ductile ASS layer into the brittle LM layer, the tensile strength of the LM layer has to be overcome, which is about three times that of ASS (see Table 1). Furthermore, when the crack is propagated from a ductile layer towards the brittle layer, initially the ductile material will absorb some of the energy, and when the crack crosses into the brittle layer its propagation is further slowed down by tractions caused by bridging of the ductile material in the wake of the crack, leading to increased toughness of the bimaterial compared to each individual component (Odette et al., 1992). The critical stress intensity factor for LM is the larger of the two materials (see Table 1), and one should hence expect to see the far field stress intensity factor to come close to or even exceed a value of $493 \pm 32$ kPa m$^{0.5}$, if the crack is introduced into the ASS layer of the beams. Taking the standard deviations of the results into account, the results seem to confirm this (see Table 3). If there was a tendency for the bimaterial to delaminate due to poor adhesion between the layers, then this phenomenon of "ductile phase toughening" would still be seen in full (Odette et al., 1992), and hence the test configuration whereby the notch is introduced into the ASS layer is not suitable for the prediction of the delamination tendencies of ASS–LM bilayer tablets.

When the crack is introduced into the brittle layer and propagates towards the ductile layer, a phenomenon called "crack arrest" is observed (Evans et al., 1989; Cao and Evans, 1991) i.e. the recorded load–deflection curves will show a pattern as shown in Fig. 6. Initially, the breaking load will rise to a first peak, at which the propagation of the crack in the brittle layer has caused failure of the brittle layer. The load then drops slightly until it is sustained by the crack that is arrested at the interface. Further bending of the beam results in an increase of the breaking load until a new crack nucleates at the interface and propagates into the ductile layer, causing final failure of the beam. This crack is not necessarily aligned with the initial notch, but can be shifted sidewise. Fig. 7 quantifies the crack arrest observed with this test configuration. The load sustained during crack arrest increased with a decrease in beam porosity in an exponential fashion. Due to the reduction in porosity the upper layer of the beams had fewer flaws and surface cracks when the bimaterials were produced at higher compaction pressures. The far field stress intensity factor is now reflecting the properties of the bimaterials rather than the properties of the ductile layer only (Cao and Evans, 1991). It can hence be compared both with the critical stress intensity factors of the individual materials obtained from experimentation (see Table 1) and the critical stress intensity factor of the interface as calculated using Eq. (3) (see above). If the bilayer tablets produced from ASS and LM have a tendency to delaminate, then the far field stress intensity factor should lie above the value obtained from Eq. (3) using ASS as the top layer (160 kPa m$^{0.5}$, see above) and below the material value for ASS ($366 \pm 12$ kPa m$^{0.5}$; see Table 1). As the far field stress intensity factor values found (see Table 3) are between 170 and 190 kPa m$^{0.5}$, it can be concluded that the combination of ASS and LM in bilayer tablets will result in delamination during storage and handling. Further evidence for this is added by comparing the values of $G_{IC}^{\infty}$ (Table 3) for this test configuration, i.e. 11.88 N/m and 13.48 N/m with the $G_{IC}^{I}$ value reported for ASS i.e. 66.2 N/m (Table 1). The $G_{IC}^{\infty}$ values are less than $0.25\times$ that of $G_{IC}^{I}$, which according to Evans and Marshall (1989) is an indication for delamination to occur during storage and handling of the specimens. As reported above, some delamination had already been observed prior to testing of the beams, confirming this conclusion. Thermal stresses due to compaction can here certainly be excluded as a main reason for the delamination tendency because of the slow compaction process. Using a similar dwell time, Buckner et al. (2010) reported temperature changes of 1.5–2.5 K only, which would probably be insufficient to cause a significant thermal stress. However, there is elastic mismatch between the materials (see Young's modulus, Table 1), and as has been explained when studying the beams

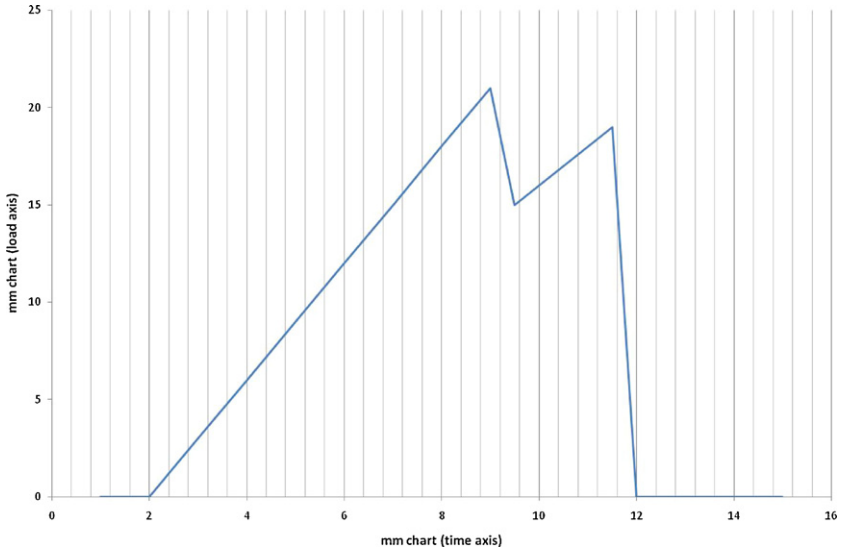


**Fig. 6.** Load–deflection curves for a bimaterial showing crack arrest during bending. The time axis is calibrated against the loading speed of the strength tester (recorder speed 200 mm/min versus bending speed 1 mm/min). The breaking load for each peak is recorded by the load cell of the strength tester and stored in the computer memory. First peak = crack propagation of the notch and fracture of the brittle layer; trough = load sustained by the crack arrested at the interface; second peak = renucleation and propagation of a crack through the top layer.

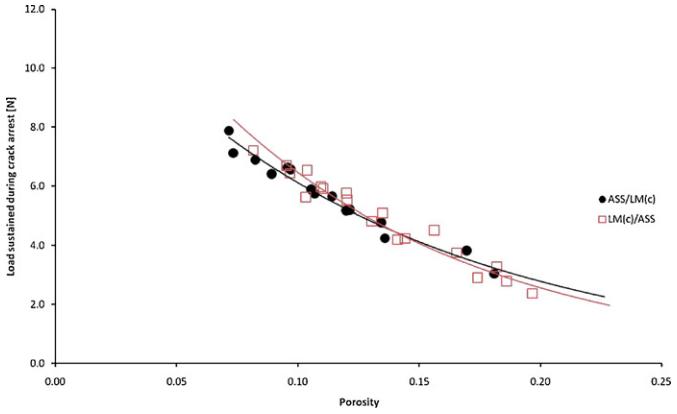


**Fig. 7.** Load sustained during crack arrest as a function of beam porosity.

made from the binary powder mixture, there is evidence that the adhesion between ASS and LM surfaces is reduced.

## 6. Conclusions

Thermal stresses due to heat development during powder compaction can result in delamination of bilayer tablets. The thermal stresses are increased for stiffer materials and can reach values well above the tensile strength of typical tablets. As a result layered tablets will delaminate. Elastic mismatch between the powders forming the individual layers will further add to the problem. The adhesion forces between ASS and LM particles and interfaces are limited, indicating a tendency for delamination of their bimaterials. It is important to identify which layer of the bimaterial behaves brittle and which one behaves ductile in order to be able to interpret the results for the far field stress intensity factor correctly. Due to ductile phase toughening it is not possible to use test configurations, where the notch is introduced into the ductile tablet layer to predict delamination tendencies. The notch must always be introduced into the brittle layer of the bimaterial i.e. in this case the LM layer. With the correct test configuration (notch in the brittle layer, which must face downward during the bending test) crack arrest at the interface was observed, and the load sustained at the interface during crack arrest increased with a decrease in beam porosity in an exponential fashion. The values obtained for the far field stress intensity factor in comparison with the critical stress intensity factor for ASS, using the correct test configuration, confirmed a strong tendency for the bimaterial to delaminate, as did the comparison between far field strain energy release rates and critical strain energy release rate for ASS. As delamination had been observed for some of the bilayer tablets, the proposed experimental test procedure is capable to predict delamination of bimaterials and could hence become a formulation tool in the development of bilayer tablets.

## References

Adams, M.J., 1985. The strength of particulate solids. J. Powder Bulk Solids Technol. 9, 15–20.
Anuar, M.S., Briscoe, B.J., 2009. The elastic relaxation of starch tablets during ejection. Powder Technol. 195, 96–104.
Anuar, M.S., Briscoe, B.J., 2010. Interfacial elastic relaxation during the ejection of bi-layered tablets. Int. J. Pharm. 387, 42–47.
Bauer, J.D., Haussühl, E., Winkler, B., Arbeck, D., 2010. Elastic properties, thermal expansion, and polymorphism of acetylsalicylic acid. Cryst. Growth Des. 10, 3132–3140.
Brown, W.F., Srawley, J.E., 1967. Plane strain crack toughness testing of high strength metallic materials. ASTM Special Technical Publ. No. 410, Am. Soc. Test. and Mater., Philadelphia.
Buckner, I.S., Friedman, R.A., Wurster, D.E., 2010. Using compression calorimetry to characterize powder compaction behaviour of pharmaceutical materials. J. Pharm. Sci. 99, 861–870.
Cao, H.C., Evans, A.G., 1991. On crack extension in ductile/brittle laminates. Acta Metall. Mater. 39, 2997–3005.
Chen, C.R., Pascual, J., Fischer, F.D., Kolednik, O., Danzer, R., 2007. Prediction of the fracture toughness of a ceramic multilayer composite – modeling and experiments. Acta Mater. 55, 409–421.
Duckworth, W., 1953. Discussion of Ryshkewitch's paper by Winston Duckworth. J. Am. Ceram. Soc. 36, 69.
Dundurs, J., 1969. Elastic interaction of dislocations with inhomogeneities. In: Mura, T. (Ed.), Mathematical Theory of Dislocations. ASME, New York, pp. 70–115.
Evans, A.G., Marshall, D.B., 1989. The mechanical behaviour of ceramic matrix composites. Acta Metall. 37, 2567–2583.
Evans, A.G., Dalgleish, B.J., He, M., Hutchinson, J.W., 1989. On crack path selection and the interface fracture energy in bimaterial systems. Acta Metall. 37, 3249–3254.
Evans, A.G., Rühle, M., Dalgleish, B.J., Charalambides, 1990. The fracture energy of bimaterial interfaces. Mater. Sci. Eng. A126, 53–64.
Gross, B., Srawley, J.E., 1965. Stress-intensity factors for three-point bend specimens by boundary collocation. Technical Note D–3092, NASA.

Gunsel, W.C., Swartz, C.J., Kanig, J.L., 1970. Tablets. In: Lachman, L., Lieberman, H.A., Kanig, J.L. (Eds.), The Theory and Practice of Industrial Pharmacy. Lea Febiger, Philadelphia, pp. 305–345.
Hassanpour, A., Ghadiri, M., Bentham, A.C., Papadopoulos, D.G., 2003. Distinct element analysis of the effect of temperature on the bulk crushing of α-lactose monohydrate. Adv. Powder Technol. 14, 427–434.
He, M.Y., Heredia, F.E., Wissuchek, D.J., Shaw, M.C., Evans, A.G., 1993. The mechanics of crack growth in layered materials. Acta Metall. Mater. 41, 1223–1228.
Heckel, W., 1961a. An analysis of powder compaction phenomena. Trans. Metal. Soc. AIME 221, 671–675.
Heckel, W., 1961b. Density–pressure relationships in powder compaction. Trans. Metal. Soc. AIME 221, 1001–1008.
Hertzberg, R.W., 1996. Deformation and Fracture Mechanics of Engineering Materials, 4th edition. Wiley, New York, pp. 280–284.
Inman, S.J., Briscoe, B.J., Pitt, K.G., 2007. Topographic characterization of cellulose bilayered tablets interfaces. Chem. Eng. Res. Des. 85, 1005–1012.
Inman, S.J., Briscoe, B.J., Pitt, K.G., Shiu, C., 2009. The non-uniformity of microcrystalline cellulose bilayer tablets. Powder Technol. 188, 283–294.
Karehill, P.G., Glaser, M., Nyström, C., 1990. Studies on direct compression of tablets. XXIII. The importance of surface roughness for the compactability of some directly compressible materials with different bonding and volume reduction properties. Int. J. Pharm. 64, 35–43.
Lacombe, R., 2006. Adhesion Measurement Methods. Theory and Practice. CRC Press, Boca Raton, pp. 155–185.
Mashadi, A.B., Newton, J.M., 1987. The characterisation of the mechanical properties of microcrystalline cellulose: a fracture mechanics approach. J. Pharm. Pharmacol. 39, 961–965.
Odette, G.R., Chao, B.L., Sheckherd, J.W., Lucas, G.E., 1992. Ductile phase toughening mechanisms in a TiAl–TiNb laminate composite. Acta Metall. Mater. 40, 2381–2389.
Phillipps, A.J., Clegg, W.J., Clyne, T.W., 1993. Fracture behaviour of ceramic laminates in bending – II. Comparison of model predictions with experimental data. Acta Metall. 41, 819–827.
Podczeck, F., 1997. Particle-particle Adhesion in Pharmaceutical Powder Handling. Imperial College Press, London, p. 169.
Podczeck, F., 2001a. Investigations into the fracture mechanics of acetylsalicylic acid and lactose monohydrate. J. Mater. Sci. 36, 4687–4693.
Podczeck, F., 2001b. The determination of fracture mechanics properties of pharmaceutical materials in mode III loading using an anti-clastic plate bending method. Int. J. Pharm. 227, 39–46.
Podczeck, F., 2002. The determination of the critical stress intensity factor in mode II loading and the shear fracture strength of pharmaceutical powder specimens. J. Mater. Sci. 37, 3595–3598.
Podczeck, F., Al-Muti, E., 2010. The tensile strength of bilayered tablets made from different grades of microcrystalline cellulose. Eur. J. Pharm. Sci. 41, 483–488.
Roark, R.J., 2002. In: Young, W.C., Budynas, R.G. (Eds.), Formulas for Stress and Strain, 7th edition. McGraw-Hill, New York, p. 17.
Roberts, R.J., Rowe, R.C., York, P., 1994. The Poisson's ratio of microcrystalline cellulose. Int. J. Pharm. 105, 177–180.
Rowe, R.C., Robert, R.J., 1995. Mechanical properties. In: Alderborn, G., Nyström, C. (Eds.), Pharmaceutical Compaction Technology. Marcel Dekker, New York, pp. 283–322.
Ryshkewitch, R., 1953. Compression strength of porous sintered alumina and zirconia. J. Am. Ceram. Soc. 36, 65–68.
Spinner, S., Knudson, F.P., Stone, L., 1963. Elastic constant porosity relations for polycrystalline theria. J. Res. Nat. Bur. Stand. C67, 39.
Stanley, P., 2001. Mechanical strength testing of compacted powders. Int. J. Pharm. 227, 27–38.
Stephenson, D., 1961. Some new aspects of tablet making. Pharm. Weekbl. 96, 689–703.
Suo, Z., Hutchinson, J.W., 1990. Interface crack between two elastic layers. Int. J. Fracture 43, 1–18.
Vaithiyalingam, S.R., Sayeed, V.A., 2010. Critical factors in manufacturing multilayer tablets – assessing material attributes, in-process controls, manufacturing process and product performance. Int. J. Pharm. 398, 9–13.
Wu, C.Y., Seville, J.P.K., 2009. A comparative study of compaction properties of binary and layered tablets. Powder Technol. 189, 285–294.
Wu, C.Y., Best, S.M., Bentham, A.C., Hancock, B.C., Bonfield, W., 2005. A simple predictive model for the tensile strength of binary tablets. Eur. J. Pharm. Sci. 25, 331–336.
York, P., Bassam, F., Rowe, R.C., Roberts, R.J., 1990. Fracture mechanics of microcrystalline cellulose. Int. J. Pharm. 66, 143–147.
Zhang, J.X., Jiang, D.L., Qin, Sh.Y., Huang, Zh.R., 2004. Fracture behaviours of laminated SiC composites. Ceram. Int. 30, 697–703.